

Article

Studies on a Thermal Fault Simulation Device and the Pyrolysis Process of Insulating Oil

Lin Du ^{1,*}, Yubo Wang ¹, Wujing Wang ² and Xiangxiang Chen ¹

¹ State Key Laboratory of Power Transmission Equipment & System Security and New Technology, Chongqing University, Chongqing 400044, China; 20143847@cqu.edu.cn (Y.W.); 1113000c@sina.cn (X.C.)

² State Grid Zhejiang Co., Ltd. Shaoxing Power Supply Company, Shaoxing 312099, China; wanglanzhu98@163.com

* Correspondence: dulin@cqu.edu.cn; Tel.: +86-138-9606-1868

Received: 3 November 2018; Accepted: 1 December 2018; Published: 4 December 2018



Abstract: In order to analyze the composition of pyrolysis products of insulating oil at different thermal fault levels, this paper proposes a thermal fault simulator device for oil-filled equipment. This device simulates different thermal fault levels by changing the heat source temperature, provides the real pressure environment by using a closed container and analyzes the composition of the insulation products by chromatographic analysis methods. By analyzing the temperature and velocity of flow distributions, it is proved that the fault simulator results are consistent with the actual results. The influence of heat source energy on the pyrolysis reaction of insulating oil is also discussed. The obtained results show that the correlation coefficient between pyrolysis product and heat source energy reaches 0.978. As a result, a multivariate nonlinear energy calculation model is presented to establish the relationship between the complete reaction process and energy. By calculating the energy absorbed by different products during the reaction, it can be found that the decomposition of alkanes absorbs a large amount of energy at the initial stage of pyrolysis, which corresponds to low temperature overheating fault. When the pyrolysis reaction continues, dehydrogenation occupies the leading role, which corresponds to high temperature overheating fault. This can be used as an effective basis for distinguishing fault levels according to the corresponding relationship between energy and fault level.

Keywords: thermal faults; mineral insulating oil; thermal fault simulator device; energy distribution

1. Introduction

Insulating oil as the main insulating material can guarantee the normal operation of the transformer [1]. Thermal faults are a common factor in destroying the insulating properties of insulating oil during transformer operation [2,3]. Therefore, the study of the pyrolysis process of insulating oil is of evident importance in the thermal fault diagnosis of transformers. Past research has focused on the effects of temperature on the pyrolysis process of insulating oils and pyrolysis products such as alkanes and alkenes [4–6]. However, energy is the direct driving force for chemical reactions. The analysis of pyrolysis reaction from the perspective of energy will make understanding of the mechanism of pyrolysis reaction more profound.

The mechanism of insulation oil pyrolysis reactions is considered as the theoretical basis of thermal fault monitoring of oil-filled equipment, consequently, attention has been paid to related research since very early. In the 1970s, Halstead deduced the chemical reaction equations and analyzed them theoretically, obtaining a model of gas production by pyrolysis of mineral oil under fault conditions [7]. Moreover, according to the calculation results of partial equilibrium pressure of different gas components, he finally proposed a Pressure-Temperature Relationship diagram. In the

1980s, Shirai put forward the two-stage decomposition theory of mineral insulating oil which divides the decomposition process of insulating oil into two stages [8]. The first stage mainly contains of the cracking reactions of alkanes; the second stage mainly contains the cracking reactions of olefins, naphthenes, and aromatic hydrocarbons. In recent years, more and more studies have been carried out on pyrolysis of organic compounds from different perspectives. Hossein and Foster studied the cracking process of oil from the point of using a multifunctional nickel catalyst [9]. Suntivarakorn studied the pyrolysis process of oil by using a circulating fluidized bed reactor [10]. Jakob and his team proposed a transformer fault diagnosis model based on chemical reaction enthalpy changes which initially explained the pyrolysis reactions of insulating oil from the angle of enthalpy change [11].

Fault simulation is one of the effective means to study the mechanism of pyrolysis reactions which can analyze the pyrolysis process from different viewpoints, such as reaction conditions, reaction environment, reaction products and so on. By quantum mechanics, Hu et al. simulated the thermal aging process of insulating paper with a Condensed-phase Optimized Molecular Potential for Atomistic Simulation Studies (COMPASS) Force Field and analyzed the effect of oxygen, water and hydrogen hydrate ions on the thermal aging degradation of insulating paper [12–14]. Yan et al. used the Reactive Force Field (ReaxFF) on the thermal aging simulation of insulating paper and cellulose by molecular reaction dynamics [15,16]. The process of dissolution was studied, and the microscopic process of fiber pyrolysis was obtained by simple analysis. Lu et al. took the lead in simulating the pyrolysis of alkanes, bicyclic alkanes, aromatic hydrocarbons and other molecules in mineral insulating oils by quantum mechanics [17]. The above fault simulation studies are all based on molecular dynamics simulation, and no experimental methods of insulation oil pyrolysis reaction were carried out, which will be highlighted in this paper.

This paper presents a thermal fault simulator for oil-filled equipment, which can be used to measure reaction energy, reaction temperature, reaction products, and so forth. Moreover, the finite element simulation model is established to verify the effectiveness of the fault simulation device. By using the thermal fault simulator for oil-filled equipment, this paper focuses on analyzing the relationship between heat source energy and products of pyrolysis reaction of insulating oil. In the end, a multivariate nonlinear energy calculation model is presented to describe this relationship.

2. Thermal Fault Simulator Description

2.1. Experimental Device

Based on the thermal faulty transformer as a prototype, the transformer thermal fault simulator is designed by proper simplification of the structure. The device is introduced separately from the housing, fault source, temperature measurement, and measurement control.

2.1.1. Enclosure

In this paper, the design of an enclosure for the sulfur hexafluoride overheating decomposition simulation device [18,19] is taken as a reference. According to the thermal fault structure, the fault volume is tiny compared with the transformer volume on the whole, and transformer oil is symmetrically distributed around the fault point. As a result, a symmetrical cylinder was chosen in the design of the enclosure shape. For the convenience of temperature and gas measurement, opening and sealing were needed on the enclosure's skirt board, and 304 stainless steel was selected as the enclosure's material. To guarantee the safety of the experiment, the inside limit pressure of the enclosure was calculated, and the thickness of the enclosure is set as 1 cm [20–22]. According to the above requirements, the parameters of the enclosure are 30 cm in diameter, 35 cm in height, 1 cm in thickness.

2.1.2. Fault Source

According to the actual faults, a fault source needs to meet three characteristics: rated power, long test time, and local heating. Given the above conditions, resistance heating was chosen as the heat source in designing the fault source, and iron flipping aluminum with a melting point of 1400 °C and a thermal conductivity of 60.2 kJ/m·h·°C was the best choice [14]. To avoid short circuits or open circuits occurring to the resistance wire in the transformer oil, aluminum oxide powder was chosen as the isolation medium among resistance coils, and stainless steel was chosen as the shell of the fault source. Alumina powder had such good insulating and thermal conductive performance [15] as the isolation material in the fault source that the heat generated by the resistance wire could come outside in time. To avoid air remaining inside the fault source, the high-pressure compressed method was adopted to evict air from the stainless steel shell. Above the stainless steel casing, the power cord led outside the enclosure through a ceramic casing with high-temperature adhesive sealing at the interfaces in transformer oil. To sum up, the heating part of the fault source was a cylinder, 2 cm in height, 6 mm in diameter.

2.1.3. Temperature Test and Control Module

Because of the significant differences in the temperature distribution around the heat source, the temperature of the internal resistance wire, the heat source surface and the area around the heat source are measured separately to observe the temperature field distribution in the oil tank and predict the severity of the fault development.

In order to measure the temperature of internal resistance wire in the fault source, a K type thermocouple was put on the surface of the resistance wire. The type K thermocouple can bear temperatures of 500 °C and its measurement precision was 0.1 °C.

To accurately measure the fault source temperature, the measurement wire of the temperature sensor temperature was fixed on the surface of the fault source and submerged in mineral insulating oil. Thus wire should be able to bear high temperatures and erosion here. A temperature measurement line with a glass fiber skin was adopted. With high transmission speed, the delay time of the glass fiber wire is just 0.2 s.

To measure the temperature of the entire cutting surface, the sensor's contacts were distributed by the upper and lower symmetry and the temperature lines were moved in parallel. According to the symmetry of the device structure, the temperature of any point around the fault source can be measured.

The sensor contacts are moved constantly, so it was necessary to use the armored type K thermocouple (WRNK-191K, Enlai Automation Technology Co., Ltd., Xiamen, China) to withstand the stress in the push-pull process. To avoid the impact on the distribution of temperature field, the contacts of the thermocouples should be moved to the wall of the enclosure after measurement. The distribution of temperature sensors in the enclosure is shown in Figure 1 [23,24].

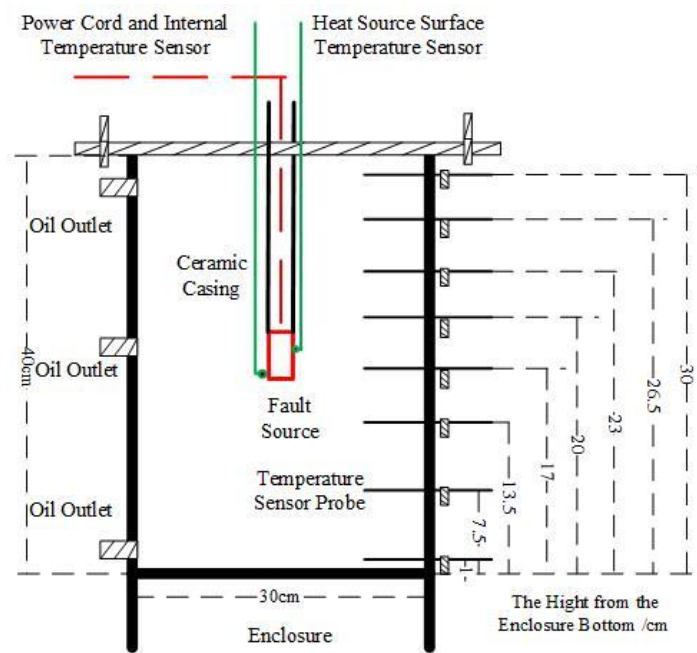


Figure 1. Temperature sensor layout.

For the control of temperature, power control was adopted in this paper. When the resistance is certain, voltage control is equivalent to control the power of the fault source. Under stable conditions, heat dissipation of the fault source to the surrounding was stable. When the thermal power and heat dissipation power of the fault source reached the equilibrium state, the temperature in the enclosure was stable. With the increase of voltage, the power of the fault source increased, and so did the stable temperature. Then thermal faults at different temperatures were simulated. The whole setup of the pyrolysis of mineral insulation oil under thermal fault conditions is shown in Figure 2.

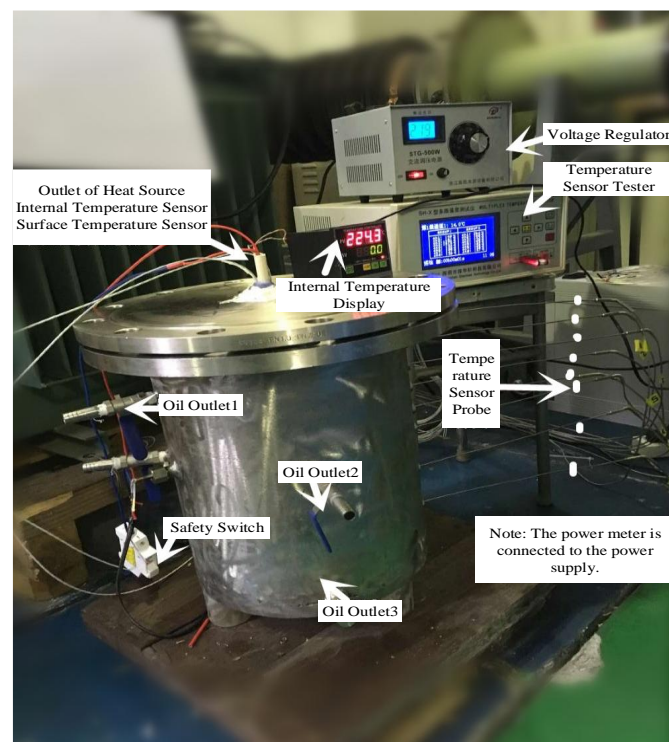


Figure 2. Pyrolysis model of mineral oil.

2.2. Experimental Process

2.2.1. Experimental Sample

DB #25 mineral insulation oil (Boshi Lubricating Oil Trading Co., Ltd., Dongguan, China), which is widely used in current transformers, was chosen as the oil sample. The important parameters of this mineral oil are shown in Table 1 below. Before the test, the sample was put in a vacuum drying oven (ZK90, Yongheng Experimental Instrument Factory, Chongqing, China) to be dried for 48 h, under the condition that pressure was 50 Pa and temperature was 90 °C. The initial moisture content of mineral oil after drying was 6 $\mu\text{L}/\text{L}$. After drying, the oil sample was put into the vacuum glove operation box (GBV-1, Zhongjing Chemical Machinery Co., Ltd., Changsha, China), filled with nitrogen and then sealed.

Table 1. Parameter list of DB#25 Mineral insulating oil.

Property	Parameter
Density (20 °C) kg/m^3	825.4
Pour Point, °C	−36
Kinematic viscosity (40 °C), mm^2/S	10.83
Acid Value, mg/g	0.03
Corrosive	non-corrosive
Water Soluble Acid or Alkali	none
Breakdown Voltage, kV	≥ 75

2.2.2. Experimental Circuit

The experimental circuit diagram is shown in Figure 3. Some steps are conducted before the experiment.

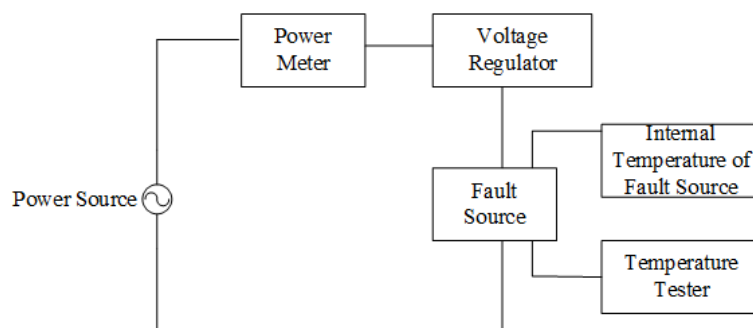


Figure 3. Experimental circuit.

1. Check the connections of the circuit

To ensure the safety of the electrical equipment, it was necessary to check the value of resistance wire in the fault source and connect a fuse in the circuit.

2. Check whether the airtight performance of enclosure was in good condition

All the oil inlets were closed, and the screws of the temperature sensor probe should ensure that the probe can be moved and no liquid seeped.

3. Prepare sampling equipment

To prevent moisture penetration, brown ground glass bottles dried 3–4 h before the test were used for sampling. After oil sampling, a rubber seal was adopted to prevent air entry which influences the test results.

2.2.3. Fault Simulation

Referring to the temperature variation regularity of internal fault and hot spots in transformer, the temperature was set at 80 °C and above and the interval was 40 °C in this paper. Put dried mineral oil in the enclosure, and set the temperature at 80 °C, 120 °C, 160 °C, 200 °C, 240 °C, 280 °C, 320 °C respectively. The oil was kept at each fault temperature for 10 h and temperatures were recorded at different distances from the fault source and the content of dissolved gas in the transformer oil was measured every hour.

2.2.4. Test the Gas Dissolved in Oil

1. Measuring equipment

The test adopted a special gc-9560-HD chromatograph produced by Shanghai Guance Electrical Technology Company (Shanghai, China). The chromatograph was equipped with a Thermal Conductivity Detector (TCD) and two Hydrogen Flame Ionization Detectors (FID). With advanced three-detector process, the chromatograph can complete the analysis of the solubility of eight kinds of gases in transformer oil in 7 min from one injection.

2. Degassing mode

The vacuum full degassing method was adopted in the experiment, and the transformer oil vacuum full degassing device JYS-5J produced by Yangzhou Huadian Electric Company (Yangzhou, China) was used. The degassing device, was also connected to the gas chromatograph online, so it can be used accurately. In this way, manual operation errors were reduced, and operation time was also saved.

3. Sampling method

Three typical locations were selected for sampling in the test: the top of the enclosure, the middle of the enclosure and the bottom of the enclosure. Three oil samples taken out from three oil outlets were measured, and the average of the measurement was finally used in the analysis. In the experiment, in order to prevent the mineral oil from spilling outside under the pressure of the gas in the enclosure, about 1–2 cm on top of the enclosure was empty, and the oil charge in it was about 25 L each time.

3. Finite Element Simulation Model

The finite element simulation model is established to study the temperature field and velocity field distribution in the tank when a thermal fault occurs. Therefore, the heat transfer relationship between insulating oil and fuel tank wall is the focus. The calculation area is set in the tank, and the boundary conditions are set according to the actual conditions. The following is the specific modeling process.

3.1. Governing Equations

When a thermal fault occurs, the heat in the tank is mainly transferred between the solid and the liquid. The way of heat transfer includes heat conduction, thermal convection, and thermal radiation. The heat generated by the heat source is mainly transferred to the insulating oil, ceramic tube and insulating adhesive. In addition, the outer surface of the tank emits little heat into the air, so it is not calculated in the model. The laminar flow equation is used to calculate the fluid heat transfer process in the insulating oil. The non-isothermal flow field is applied to the oil tank because of the surge of insulating oil during the heating process. Meanwhile, the temperature field is regarded as the coupling field of laminar flow and non-isothermal flow.

The heat transfer equation for solids is [25,26]:

$$\rho C_p \frac{\partial T}{\partial t} + \rho C_p u \cdot \nabla T + \nabla \cdot q = Q + Q_{ted} \quad (1)$$

$$q = -k\nabla T \quad (2)$$

The laminar flow equation for a liquid is [27]:

$$\rho \frac{\partial u}{\partial t} + \rho(u \cdot \nabla)u = \nabla \cdot \left[-\rho I + \mu(\nabla u + (\nabla u)^T) \right] + F\rho \nabla \cdot (u) = 0 \quad (3)$$

where ρ is the density of solid, C_p is the normal pressure heat capacity, u is the convective velocity, T is the surface temperature of solid, q is the convective heat flux, Q and Q_{rad} are the initial energy and the radiation energy of solid, respectively, F is the volume force and I is linear inertia force.

3.2. Boundary Condition Setting and Calculation Realization

In the test, the power of the heat source is set to 50, 100, 150, 200, 250, and 300 W and so on, which simulates the development of the thermal fault under different temperature and different power. When the constraint value of the pressure point is set to the port, the initial value is 0. The initial temperature is set to 293.15 K, and the velocity field and initial pressure are set at 0.

In the numerical simulation model, the heat transfer process in the tank is simplified to a 2D model because of its axisymmetric structure. Reasonable mesh generation is essential for the accurate solution of numerical simulation models [28,29]. Therefore, for the 2D model, the scanning network partition method is adopted. The vicinity of the heat source is preferentially divided into more detailed sections, and the grid is then swept to the tank boundary. The final partition network is obtained as shown in Figure 4. The quality of the smallest and average elements is 0.8536 and 0.9868, respectively, which ensures the accuracy of the calculation results. The final calculation process is shown in Figure 5 [30].

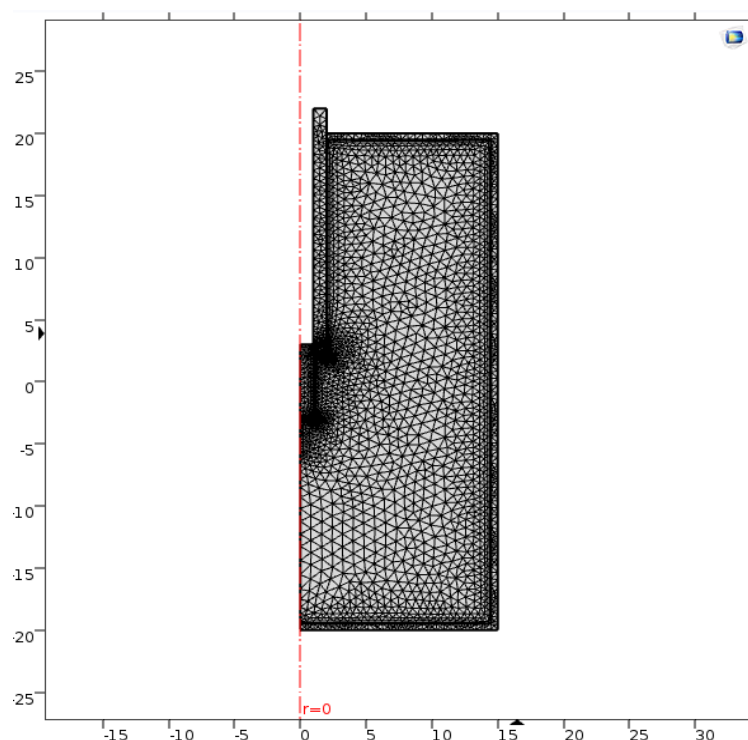


Figure 4. Diagram of mesh.

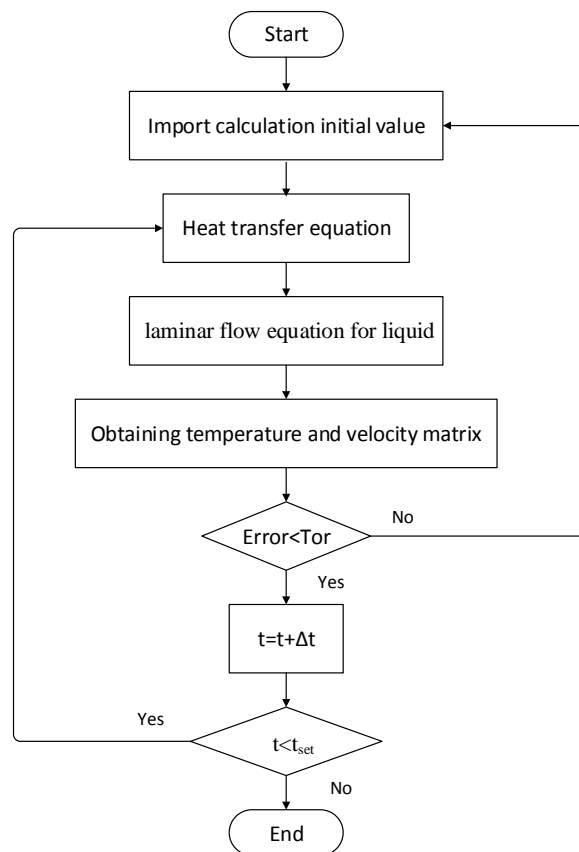


Figure 5. Calculation flow chart.

4. Experimental Result and Analysis

4.1. Temperature Field Distribution of Oil Tank in Fault Simulation Experiment

In the fault simulation device, based on the height of the temperature sensor and the distance of the probe from the heat source, a cylindrical coordinate system can be established to measure the temperature in different positions in the oil tank. Because the fault simulation device is an axisymmetric structure, the temperature of the temperature sensor in the same height and the same distance from the heat source is approximately equal, so the temperature field can be seen as a variable related to height and distance from the heat source. In the fault simulation device, five feature points are selected, and the temperature of the five feature points is detected for a long time. Finally, the relationship between the temperature of the feature points and the time is shown in Figure 6. Among them, (17, 0) points are the surface points of the heat source, and (17, 0.5) points represent the characteristic points where is 5 cm away from the heat source. The (1, 0) point represents the lowest point of the fault simulation device directly below the heat source. (20, 0.5), (23, 0.5) indicate the point where its lateral distance from the heat source is 5 cm, and the distance from the bottom surface of the fault simulation device is 20 and 23 cm respectively. Based on the plot of temperature vs. time for feature points, the following conclusions can be drawn:

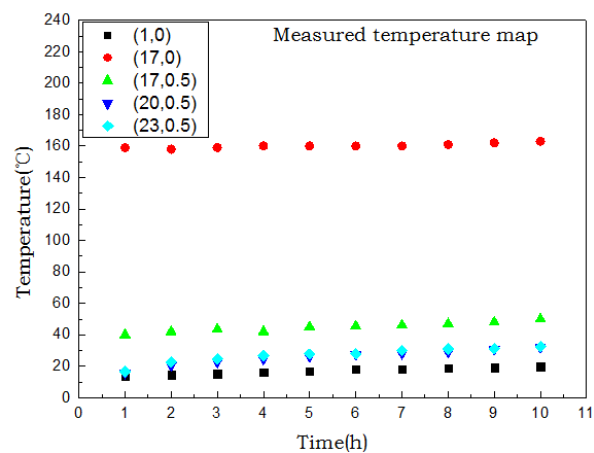


Figure 6. The temperature of each point in the experimental device when the heating temperature is 160 K.

By observing the change in temperature of the three feature points at a distance of 5 cm from the heat source, it can be found that the temperature rises slowly, which shows that the fault simulation device works well for the heating and fault simulation of mineral insulating oil near the heat source, but the heating temperature far from the heat source cannot reach the ideal value, which is in line with the finite element simulation results in Figure 7. This is consistent with the fact that the temperature at the winding in the transformer tank is significantly higher than the oil temperature at the far point [31]. Therefore, we conclude that the fault simulation device can be more realistic to restore the trend of temperature changes in the transformer oil tank when a thermal fault occurs.

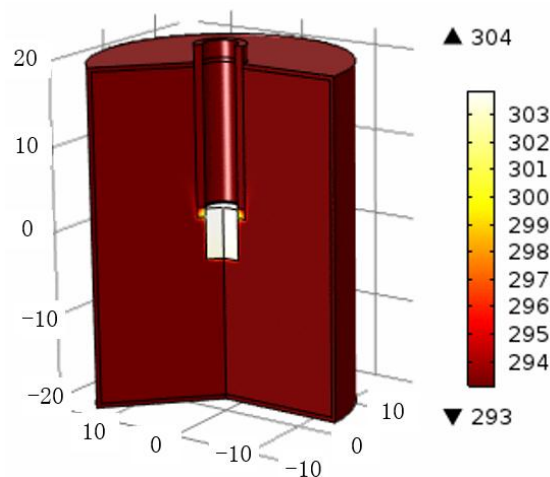


Figure 7. Temperature field distribution of finite element simulation model.

4.2. Pyrolysis Gas Production of Insulating Oil in Fault Simulation Experiment

It can be seen from the Figure 8 that when the heating temperature is 80 °C, methane is generated first, and the content of methane increases significantly with increasing temperature, which is in accordance with the pyrolysis law of mineral insulation oil under actual fault conditions [7]. When the heating temperature reaches 120 °C, ethane gas is generated, yet when the temperature reaches 160 °C, the content of ethane gas decreases, while ethylene gas is produced. With the temperature rising to 240 °C, the content of ethylene keeps rising, while the content of ethane does not change substantially between 200 °C and 240 °C. This is because insulation oil preferentially undergoes the chain scission reaction of paraffins in the event of a low-temperature fault, and changes from long-chain paraffins to short-chain paraffins [4]. Therefore, methane gas and ethane gas are generated first. As the temperature

reaches the mid-temperature fault condition, some short-chain paraffins undergo simultaneous chain scission and dehydrogenation reactions, including partial ethane gas dehydrogenation reactions to produce ethylene, so a large increase in the content of methane occurs, and the content of ethylene decreases. When the oil is heated from 240 °C to 280 °C, the ethylene content is reduced significantly, while acetylene gas is generated and the content is greatly increased, which indicates that the mineral insulating oil undergoes the second stage reaction, the olefin undergoes dehydrogenation during the heating process and alkynes are produced [9].

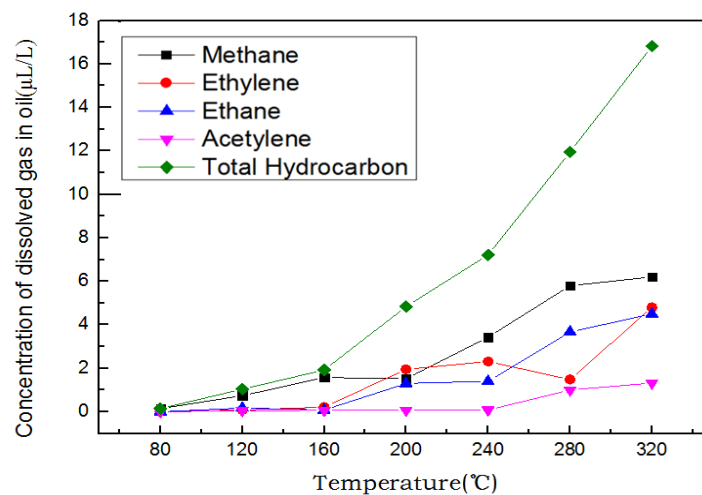


Figure 8. Change of the gas content under different temperatures.

Combining with the above results and previous studies [1–4], the pyrolysis process of insulating oil can be established. When mineral oil is overheated at low temperature, the bond breaking and dehydrogenation of alkane molecules occur first. The bond breaking reaction mainly refers to the chain breaking of C_{20} alkane and the formation of small molecules such as C_1 – C_4 and C_{10} – C_{19} . At the same time, dehydrogenation reactions occur. The carbon-carbon bonds in the C_{20} molecule dehydrogenate to produce carbon-carbon double bonds and hydrogen. With the increase of temperature, C_{10} – C_{19} hydrocarbon molecules decompose further to produce small molecules such as C_1 – C_4 and C_4 – C_9 , accompanied by the dehydrogenation of C_{10} – C_{19} hydrocarbon molecule. As the temperature continues to rise, naphthenes and aromatic hydrocarbon molecules in the mineral oil decompose, accompanied by bond breaking and dehydrogenation of small molecules such as C_4 – C_9 . When the insulating oil reaches a high temperature level, the olefins in the system dehydrogenate to form alkynes. At this time, the mineral insulating oil completes the thermal decomposition process. The pyrolysis process of insulating oil is shown in Figure 9.

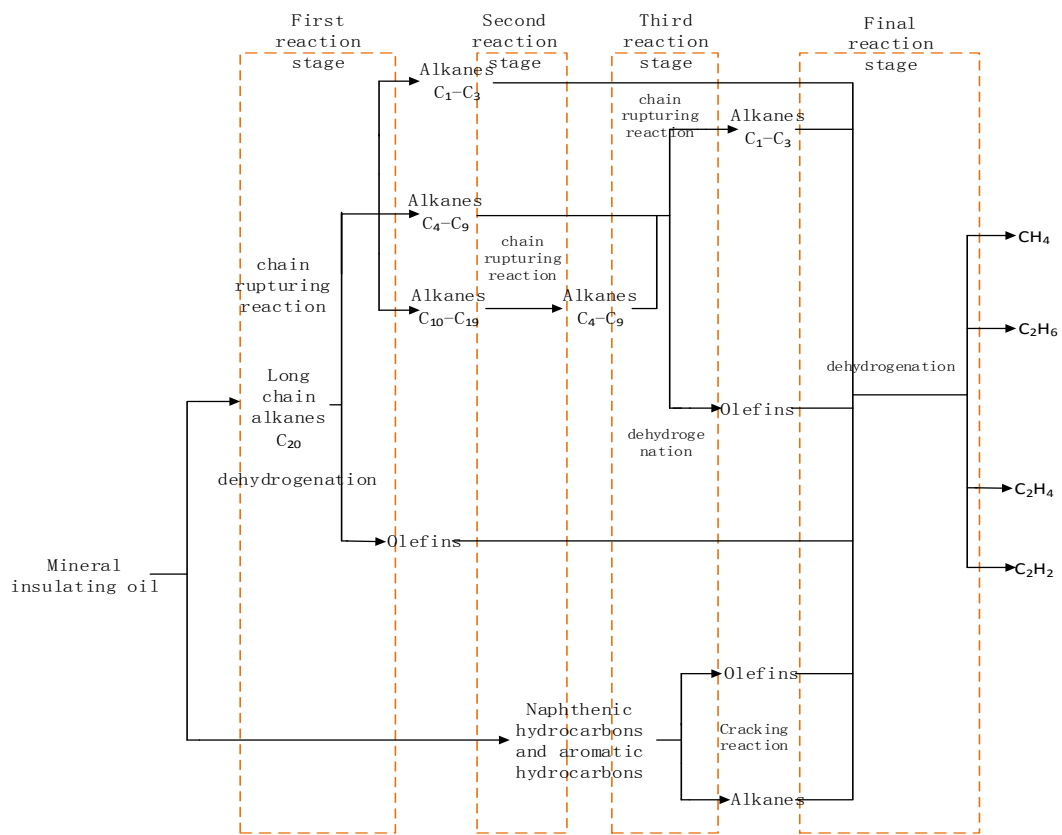


Figure 9. The pyrolysis process of insulating oil.

4.3. Relationship between Heat Source Energy and Pyrolysis Reaction of Insulating Oil

The output voltage of the AC voltage source is adjusted to change the heating power of the heat source so that the temperature sensors on the resistance wires are 80, 120, 160, 200, 240, 280, 320, respectively. The insulation oil in the fault simulator is continuously heated for 10 h. The oil samples are taken from the oil tank for thermal spectrum analysis and detection, and the various gases in the oil are recorded. The average heating power of 10 h is calculated by reading the power meter in the circuit every 1 h. Hence, the energy released from the heat source can be obtained by calculating the heating time and the average heating power of the heat source. Figure 10 describes the relationship between the heat release energy and the content of various gaseous components in the oil.

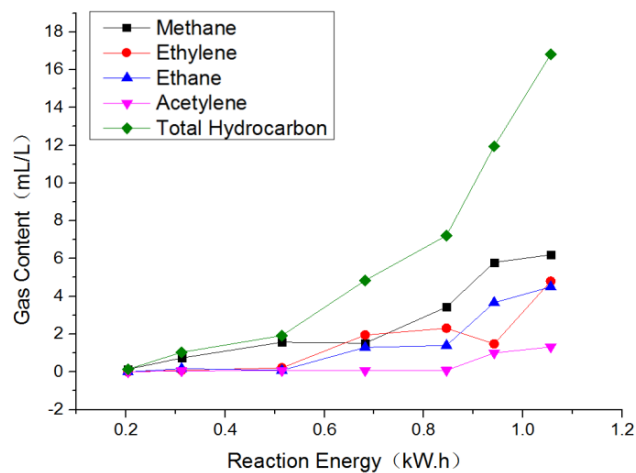


Figure 10. Change of the gas content under different energy.

In Figure 10, it is shown that the pyrolysis gas content of mineral insulating oil changes significantly with the release of heat energy. The content of methane increases when the heat energy is low. However, with the increase of heat source energy, the content of methane does not change until the heat source energy reaches 0.7 kWh, and the content of methane gas rises again. According to the two-stage pyrolysis theory of mixed insulating oil [4] combined with our analysis, when the heating energy of heat source is low, it can be deduced that alkane chains are broken to produce methane, while the methane gas content increases again because of the decomposition reaction of naphthenes and aromatic hydrocarbons in the mineral insulating oil. The constant content of methane is due to the fact that the heating energy of the heat source does not reach the activation energy of the decomposition reaction. The content of ethane increases first with the increase of energy then remains stable, and finally increases again. This changing trend is consistent with the change trend of methane, which accurately reflects the general change trend and the main reaction process of alkane gases in the case of increasing energy. At the same time, when the heating energy of the heat source is 0.5 kWh, ethylene is produced. When the heating energy reaches 0.85 kW, it can be found that the content of ethylene decreases significantly, while acetylene is produced, which indicates that the heat source release energy reaches the reaction activation energy of olefin dehydrogenation. Consequently, the dehydrogenation reaction takes place, resulting in the reduction of ethylene and the increase of acetylene. In conclusion, it can be deduced that the energy needed for chain breaking reaction of long chain alkane is 0.2–0.5 kWh per liter of insulating oil. The energy for decomposition of naphthenic hydrocarbons and aromatic hydrocarbons is 0.5–0.7 kWh per liter of insulating oil. The energy for dehydrogenation reaction of carbon-carbon double bond is 0.85–0.95 kWh per liter of insulating oil. The chemical reaction energy obtained is recorded in Table 2.

Table 2. Chemical reaction energy table.

Chemical Reaction	Energy (kWh/L)
$C_{20} \rightarrow C_1-C_9 + C_{10}-C_{19}$	0.2–0.5
Unsaturated hydrocarbons \rightarrow olefins + alkynes	0.5–0.7
olefins + alkanes \rightarrow acetylene + hydrogen	0.85–0.95

4.4. Multivariate Nonlinear Energy Calculation Model and Result Analysis

According to the above analysis, it is evident that there is a quantitative relationship between heat source energy and pyrolysis gas output. Some authors have proposed a multivariate linear model to describe the relationship, which is derived based on the enthalpy theory [32,33]. Yet, the model is not entirely consistent with the development of pyrolysis reaction due to the complexity of organic reactions. To establish the relationship between the complete reaction process and energy, the multivariate nonlinear energy calculation model is presented. In order to properly simplify the model, the following conditions are assumed:

- The content of methane, ethane, ethene and acetylene in pyrolysis is higher than that of other products.
- Most of the heat energy is converted to chemical reaction energy, and energy dissipation is ignored.
- Hydrogen occurs in a variety of organic reactions, making the product's contribution to energy duplicate, so hydrogen is not selected as the characteristic gas.

In the multivariate nonlinear energy calculation model, a three degree polynomial is used to describe the energy absorbed by the production of hydrocarbons. Methane, ethane, ethylene, and acetylene are selected as characteristic gases to estimate the heat source energy, because they are significantly more abundant than other products. The measurement of model parameters is very difficult due to various parameters and independent variables. A Particle Swarm Optimization algorithm is used because it can start from random solutions and find the optimal solution by iteration. The number of population, the number of neighboring population, and the learning factor are set to 50,

2, and 2.05 respectively for accuracy. As a result, the multivariate nonlinear energy estimation model was built as follows:

$$y = 249.9x_1 - 10x_1^2 - 7.4x_1^3 + 47x_2 - 13.67x_2^2 + 9.83x_2^3 + 112x_3 - 7.9x_3^2 - 35x_3^3 + 2566.5x_4 + 33.86x_4^2 + 22.87x_4^3 \tag{4}$$

where y is the heat source energy, x_1 , x_2 , x_3 and x_4 are the contents of methane, ethylene, ethane and acetylene respectively.

The calculated values and actual values of heat sources are shown in Figure 11. It can be seen that the estimated value of energy is basically consistent with the actual value. The correlation coefficient reached 0.978. Nevertheless, at the initial stage of pyrolysis, there is still a gap between the estimated energy and the actual value. At the early stage of pyrolysis, the content of pyrolysis products is small, and the energy lost cannot be ignored, which leads to this error. At the same time, the heat absorption of ethylene and acetylene in the pyrolysis reaction calculated by a multivariate nonlinear model is shown in Figure 12.

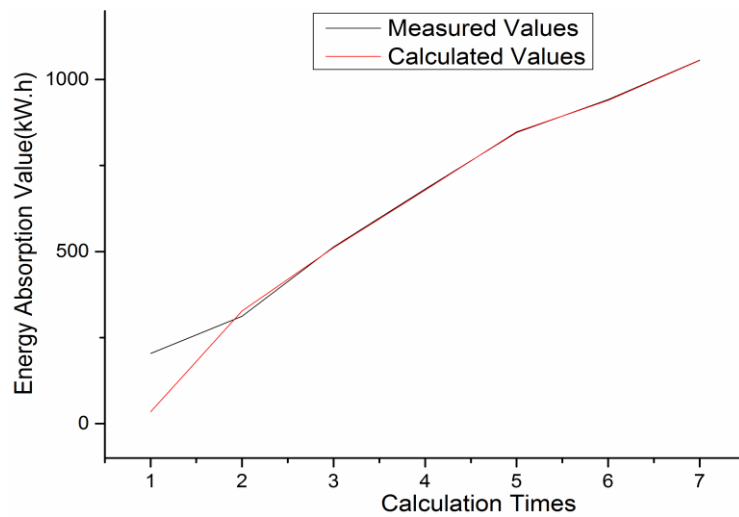


Figure 11. Result comparison diagram.

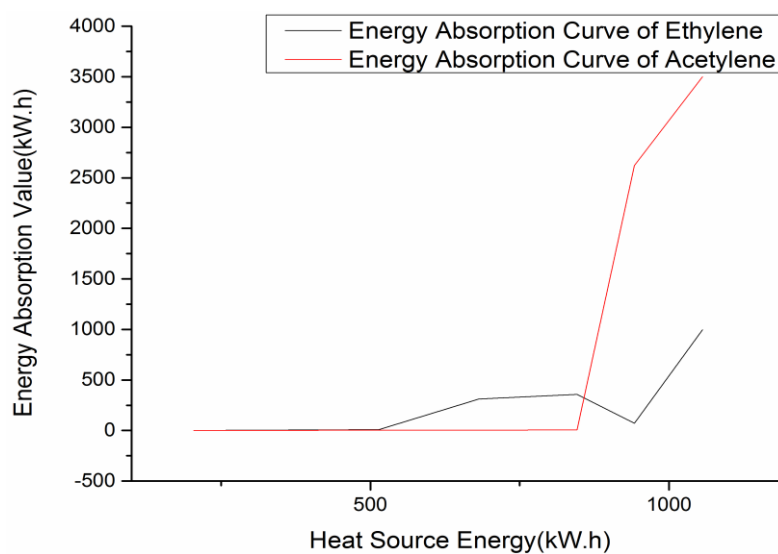


Figure 12. Energy absorption curve.

In Figure 11, it can be seen that the energy absorbed by ethylene increases gradually during the initial stage of the pyrolysis reaction, corresponding to the chemical reaction of dehydrogenation of alkanes to olefins. This indicates that a large number of carbon-carbon single bonds dehydrogenate to form carbon-carbon double bonds at this stage. As the heat source energy continues to rise, the energy absorption curve of ethylene decreases, and the energy absorption curve of acetylene increases, which proves that the dehydrogenation of alkanes and olefins takes place at the same time, and the olefin content as the reactant is more than the olefin content produced. Carbon-carbon double bonds dehydrogenate at this stage to form carbon-carbon triple bonds. In the final stage of the reaction, the energy absorption curves of ethylene and acetylene rise simultaneously, which is thought to be a large amount of energy absorbed by the decomposition reaction of naphthenic hydrocarbons and aromatic hydrocarbons [1]. As a result, the reaction energy for cracking reaction of paraffins is 0.2–0.5 kWh per liter of insulating oil. The reaction energy of dehydrogenation reaction is 0.5–1 kWh per liter of insulating oil, which is consistent with the conclusion of the last section. The energy values calculated by nonlinear energy calculation model are also consistent with previous studies on the pyrolysis of insulating oils and are considered to be effective in estimating the pyrolysis reaction at any stages.

5. Conclusions

A thermal fault simulator for oil-filled equipment is presented in detail and a multivariate nonlinear energy calculation model is proposed in the paper. The conclusions are as follows:

1. The fault simulator can simulate the pyrolysis process of the insulated oil well through the comparison of the experimental results with the two-stage pyrolysis theory proposed by Shirai [2].
2. Further analysis of the heating process of the insulating oil indicates that the pyrolysis process of the insulating oil is gradually completed. Different pyrolysis stages correspond to different reactions and products. According to this analysis, a pyrolysis path model for insulating oil is obtained.
3. A multivariate nonlinear energy calculation model is proposed, which provides a way to calculate the reaction energy through the pyrolysis products of insulating oils.
4. The heat source energy required for different pyrolysis processes is calculated by the multivariate nonlinear energy calculation model.

In general, the transformer thermal fault simulator can be used as a test platform for transformer thermal fault research. Its experimental results have certain reference significance. Moreover, the multivariate nonlinear energy calculation model can be used as a new method to analyze and define the stages of thermal failure, which establishes a bridge to deeply understand the relationship between the complete reaction process and energy.

Author Contributions: Conceptualization, L.D. and Y.W.; methodology, L.D. and Y.W.; software, W.W., L.D. and Y.W.; validation, L.D., Y.W. and X.C.; formal analysis, Y.W.; investigation, X.X.; resources, L.D.; data curation, W.W.; writing—original draft preparation, X.C.; writing—review and editing, L.D. and Y.W.; visualization, X.C.; supervision, W.W.; project administration, L.D.; funding acquisition, L.D.

Funding: This research received no external funding.

Conflicts of Interest: The authors declare no conflict of interest.

References

1. Gabbar, H.A.; Aboughaly, M.; Stoute, C.B. DC Thermal Plasma Design and Utilization for the Low Density Polyethylene to Diesel Oil Pyrolysis Reaction. *Energies* **2017**, *10*, 784. [[CrossRef](#)]
2. Zou, J.; Chen, W.; Wan, F.; Fan, Z.; Du, L. Raman Spectral Characteristics of Oil-Paper Insulation and Its Application to Ageing Stage Assessment of Oil-Immersed Transformers. *Energies* **2016**, *9*, 946. [[CrossRef](#)]
3. Wu, J.; Li, K.; Sun, J.; Xie, L. A Novel Integrated Method to Diagnose Faults in Power Transformers. *Energies* **2018**, *11*, 3041. [[CrossRef](#)]

4. Xun, H.; Hongyu, G.; Mortaza, G.; Behnam, S.; Qing, L. Pyrolysis of Different Wood Species: Impacts of C/H Ratio in Feedstock on Distribution of Pyrolysis Products. *Biomass Bioenergy* **2019**, *120*, 28–39.
5. Agblevor, F.A.; Jahromi, H. Aqueous Phase Synthesis of Hydrocarbons from Reactions of Guaiacol and Low Molecular Weight Oxygenates. *ChemCatChem* **2018**, *10*, 1102. [[CrossRef](#)]
6. Foster, A.A.; Hossein, J. Aqueous-Phase Synthesis of Hydrocarbons from Furfural Reactions with Low-Molecular-Weight Biomass Oxygenates. *Energy Fuel*. **2018**, *32*, 8552–8562.
7. Halstead, W.D. A Thermodynamic Assessment of the Formation of Gaseous Hydrocarbons in Faulty Transformers. *J. Inst. Pet.* **1973**, *59*, 239–241.
8. Shirai, M.; Shimoji, S.; Ishii, T. Thermodynamic Study on the Thermal Decomposition of Insulating Oil. *Electr. Insul.* **1977**, *12*, 272–280. [[CrossRef](#)]
9. Hossein, J.; Foster, A.A. Hydrodeoxygenation of Aqueous-Phase Catalytic Pyrolysis Oil to Liquid Hydrocarbons Using Multifunctional Nickel Catalyst. *Ind. Eng. Chem. Res.* **2018**, *57*, 13257–13268.
10. Suntivarakorn, R.; Treedet, W.; Singbua, P.; Teeramaetawat, N. Fast Pyrolysis from Napier Grass for Pyrolysis Oil Production by Using Circulating Fluidized Bed Reactor: Improvement of Pyrolysis System and Production Cost. *Energy Rep.* **2018**, *4*, 565–575. [[CrossRef](#)]
11. Jakob, F.; Noble, P.; Dukarm, J.J. A Thermodynamic Approach to Evaluation of the Severity of Transformer Faults. *IEEE Trans. Power Deliv.* **2012**, *27*, 554–559. [[CrossRef](#)]
12. Wang, X.; Tang, C.; Wang, Q.; Li, X.; Hao, J. Selection of Optimal Polymerization Degree and Force Field in the Molecular Dynamics Simulation of Insulating Paper Cellulose. *Energies* **2017**, *10*, 1377. [[CrossRef](#)]
13. Liao, R.J.; Hu, S.; Yang, L.J. Molecular Simulation of Micro-mechanism of Thermal Aging Degradation of Transformer Insulation Paper. *High Volt. Technol.* **2009**, *35*, 1565–1570.
14. Yuan, Q.; Hu, S.; Zhou, T.C. Experimental Study on Temperature Response to Frequency Domain Dielectric Ageing of Oil-paper Insulation for Transformers. *High Volt. Electr. Appar.* **2013**, *2*, 74–79.
15. Yan, J.Y.; Wang, X.L.; Li, Q.M. Molecular Dynamics Simulation of High Temperature Pyrolysis of Insulating Paper. *Chin. J. Electr. Eng.* **2015**, *35*, 5941–5949.
16. Krishnan, Y.; Byrne, A.; English, N.J. Vibrational Study of Iodide-Based Room-Temperature Ionic-Liquid Effects on Candidate N719-Chromophore/Titania Interfaces for Dye-Sensitised Solar-Cell Applications from Ab-Initio Based Molecular-Dynamics Simulation. *Energies* **2018**, *11*, 2570. [[CrossRef](#)]
17. Liao, R.J.; Lu, Y.C.; Yang, L.J. Simulated Calculation of Space Charge Trap Depth in Polymer Dielectrics. *Insul. Mater.* **2006**, *39*, 51–54.
18. Wang, Y.; Li, L.; Yao, W. Analysis and Discussion of SF₆ Byproducts in Simulated Electric Equipment of Overheating Faults in Low Humidity. *Phys. Rev. Lett.* **2011**, *106*, 1–3.
19. Tang, J.; Huang, X.J.; Xie, Y.B. Design and Establishment of Experimental Simulation System Concerning SF₆ Thermal Decomposition. *High Volt. Eng.* **2014**, *40*, 3388–3395.
20. Ding, B.; Cai, R.L. *Principles of Pressure Vessel Design and Engineering Applications*; Machinery Industry Press: Beijing, China, 1987.
21. Huang, J.S. *Special Material for Practical Application of Pressure Vessel Materials*; Chemical Industry Press: Beijing, China, 1983.
22. Castello, D.; Rolli, B.; Kruse, A.; Fiori, L. Supercritical Water Gasification of Biomass in a Ceramic Reactor: Long-Time Batch Experiments. *Energies* **2017**, *10*, 1734. [[CrossRef](#)]
23. Amoiralis, E.I.; Tsili, M.A.; Kladas, A.G. Transformer Design and Optimization: A Literature Survey. *Power Deliv. IEEE Trans. Power Deliv.* **2009**, *24*, 1999–2024. [[CrossRef](#)]
24. Li, Y.; Yan, Z.; Yang, C.; Guo, B.; Yuan, H.; Zhao, J.; Mei, N. Study of a Coil Heat Exchanger with an Ice Storage System. *Energies* **2017**, *10*, 1982. [[CrossRef](#)]
25. Henshaw, W.D.; Chand, K.K. A Composite Grid Solver for Conjugate Heat Transfer in Fluid-structure Systems. *J. Comput. Phys.* **2009**, *228*, 3708–3741. [[CrossRef](#)]
26. Yu, L.-H.; Xu, S.-X.; Ma, G.-Y.; Wang, J. Experimental Research on Water Boiling Heat Transfer on Horizontal Copper Rod Surface at Sub-Atmospheric Pressure. *Energies* **2015**, *8*, 10141–10152. [[CrossRef](#)]
27. Thomas, S.K.; Lykins, R.C.; Yerkes, K.L. Fully Developed Laminar Flow in Trapezoidal Grooves with Shear Stress at the Liquid—Vapor Interface. *Int. J. Heat Mass Transf.* **2001**, *44*, 3397–3412. [[CrossRef](#)]
28. Jia, C.; Ji, L.; Yu, Z. Fluid Model of Inductively Coupled Plasma Etcher Based on COMSOL. *J. Semicond.* **2010**, *31*, 19–24. [[CrossRef](#)]

29. Yang, Y.; El Baghdadi, M.; Lan, Y.; Benomar, Y.; Van Mierlo, J.; Hegazy, O. Design Methodology, Modeling, and Comparative Study of Wireless Power Transfer Systems for Electric Vehicles. *Energies* **2018**, *11*, 1716. [[CrossRef](#)]
30. Hosseinzadeh, E.; Marco, J.; Jennings, P. Electrochemical-Thermal Modelling and Optimisation of Lithium-Ion Battery Design Parameters Using Analysis of Variance. *Energies* **2017**, *10*, 1278. [[CrossRef](#)]
31. Jiang, T.S.; Li, J.; Chen, W.G. Heat circuit model for calculating hot spot temperature of oil-immersed transformer windings. *High Volt. Technol.* **2009**, *35*, 1635–1640.
32. Sun, C.X.; Chen, W.G.; Li, J. *Electrical Equipment Dissolved Gases On-Line Monitoring and Fault Diagnosis Technology*; Science Press: Beijing, China, 2003.
33. Wang, X.L.; Li, Q.M.; Yang, R. Multi Index Comprehensive Weight Assessment Method for Transformer Composite Insulation Defects Based on Oil Chromatogram Analysis. *High Volt. Technol.* **2015**, *41*, 3836–3842.



© 2018 by the authors. Licensee MDPI, Basel, Switzerland. This article is an open access article distributed under the terms and conditions of the Creative Commons Attribution (CC BY) license (<http://creativecommons.org/licenses/by/4.0/>).